Available online at www.sciencedirect.com
ScienceDirect
Lithos 92 (2006) 506–523
LITHOS
www.elsevier.com/locate/lithos

Exsolution textures in orthopyroxene in aluminous granulites as indicators of UHT metamorphism: New evidence from the Eastern Ghats Belt, India

Sankar Bose [a], Kaushik Das [b], Somnath Dasgupta [c,*], Hiroyuki Miura [d], Masato Fukuoka [e]

[a] *Department of Geology, Presidency College, Kolkata-700 073, India*
[b] *Department of Applied Geology, Indian School of Mines, Dhanbad-826004, India*
[c] *Department of Geological Sciences, Jadavpur University, Kolkata-700 032, India*
[d] *Department of Earth and Planetary Sciences, Hokkaido University, Sapporo 060, Japan*
[e] *Department of Earth and Planetary Sciences, Faculty of Integrated Arts and Science, Hiroshima University, Higashi-Hiroshima 724, Japan*

Received 27 May 2005; accepted 30 March 2006
Available online 30 June 2006

Abstract

Highly aluminous orthopyroxene, coexisting with sapphirine, cordierite, sillimanite, quartz and garnet in various combinations, constitute granoblastic mosaic peak metamorphic assemblages in aluminous granulites from three localities in the Eastern Ghats Belt, India. Orthopyroxene contains four types of intergrowths: (a) involving sapphirine with or without cordierite, (b) involving spinel, but without sapphirine, (c) involving cordierite, but without sapphirine and spinel, and (d) involving garnet, without sapphirine, spinel or cordierite. On the basis of textural and compositional data, origin of the intergrowths is ascribed to breakdown of Mg-Tschermak component, locally also involving Fe- and Ti-Tschermak. An attempt is made to compute the "pre-breakdown" compositions of orthopyroxene by image analysis, which shows maximum Al_2O_3 content of 13.4 wt.% in the pristine orthopyroxene. Geothermometry, phase equilibria consideration and application of existing experimental data on alumina solubility in orthopyroxene coexisting with sapphirine and quartz, collectively indicate extreme thermal conditions of metamorphism (>1000 °C) for the studied assemblages. This re-affirms the notion that Al_2O_3 solubility in orthopyroxene is the most powerful indicator of UHT metamorphism (Harley, S.L., 2004. Extending our understanding of ultrahigh temperature crustal metamorphism. J. Mineral. Petrol. Sci. 99, 140–158). The intergrowths are considered to have formed due to cooling from the thermal peak spanning a temperature range of approximately 150 °C. Appearance of diverse types of intergrowths is probably related to subtle differences in bulk composition, particularly Fe:Mg ratios.

Keywords: Eastern ghats; UHT metamorphism; Aluminous orthopyroxene; Intergrowth textures

1. Introduction

Ultra-high temperature metamorphosed pelitic granulites the world over contain highly aluminous orthopyroxene as a major constituent, coexisting with sapphirine,

* Corresponding author. Tel.: +91 33 2416 6781; fax: +91 33 2416 6484.
E-mail address: somnathdg@rediffmail.com (S. Dasgupta).

0024-4937/$ - see front matter © 2006 Elsevier B.V. All rights reserved.
doi:10.1016/j.lithos.2006.03.062

quartz, spinel, sillimanite, garnet, osumilite and cordierite (reviewed in Harley, 1989, 1998, 2004). Experimental data in parts of the system KFMASH under extreme thermal conditions (Carrington and Harley, 1995; Das et al., 2001, 2003) have supported the natural observation that orthopyroxene in UHT metapelitic granulites is highly aluminous, caused by extensive Tschermak substitutions. As emphasized by Harley (2004), the highly aluminous nature of orthopyroxene coexisting with sapphirine, quartz, sillimanite or garnet provides the most powerful indicator of UHT metamorphism. It is now possible to quantify peak metamorphic thermal conditions from alumina solubility in orthopyroxene when other conventional thermometers have doubtful application (e.g. Harley and Motoyoshi, 2000). Although attempts have been made to retrieve peak thermal conditions by formulating Fe–Mg exchange thermometers that use a feedback mechanism (Fitzsimons and Harley, 1994; Pattison et al., 2003), the alumina solubility in orthopyroxene, monitored by several Tschermak exchange vectors, remains as an important UHT sensor.

The Proterozoic Eastern Ghats Belt (EGB) in India is one of the key terrains that experienced UHT metamorphism at lower crustal levels (Dasgupta, 1995; Dasgupta and Sengupta, 2003; Dobmeier and Raith, 2003, references therein). Several varieties of ortho- and paragneisses, basic and ultrabasic intrusives constitute the lithological ensemble of the EGB (Dasgupta, 1995). UHT metamorphism has been documented largely from the study of metapelitic aluminous granulites and calc-silicate granulites (Dasgupta and Sengupta, 1995, 2003). The aluminous granulites represent both pelitic and semipelitic protoliths (Lal et al., 1987; Sengupta et al., 1990; Dasgupta et al., 1995; Bose et al., 2000). Orthopyroxene is a part of the peak metamorphic assemblage in most of the occurrences of such aluminous granulites in the EGB, and, like other UHT terrains, is highly aluminous (8–12 wt.% Al_2O_3) (Dasgupta and Sengupta, 2003; Sarkar et al., 2003). In this communication, we describe a plethora of intergrowth textures in such orthopyroxenes from three localities in the EGB, and attempt to model their origin in the background of the already established UHT metamorphism and retrograde *P–T* paths of this belt. All mineral abbreviations used are after Kretz (1983).

2. Geological background

The studied aluminous granulite occurrences are near Araku, Vishakhapatnam District of Andhra Pradesh, India (Fig. 1). Samples for the present study were collected from three localities Sunkarametta (SS), (N18°16′36″, E82°58′6″), Loteru (9d and Lnd), (N18°19′36″, E83°4′22″) and Panirangini (Pan) (N18°18′26″, E82°54′25″) (Fig. 1). Out of these, Sunkarametta area has been previously studied by Bose et al. (2000). Aluminous granulites occur characteristically as enclaves of variable dimension within quartzofeldspathic and pelitic gneisses. At Sunkarametta, these enclaves

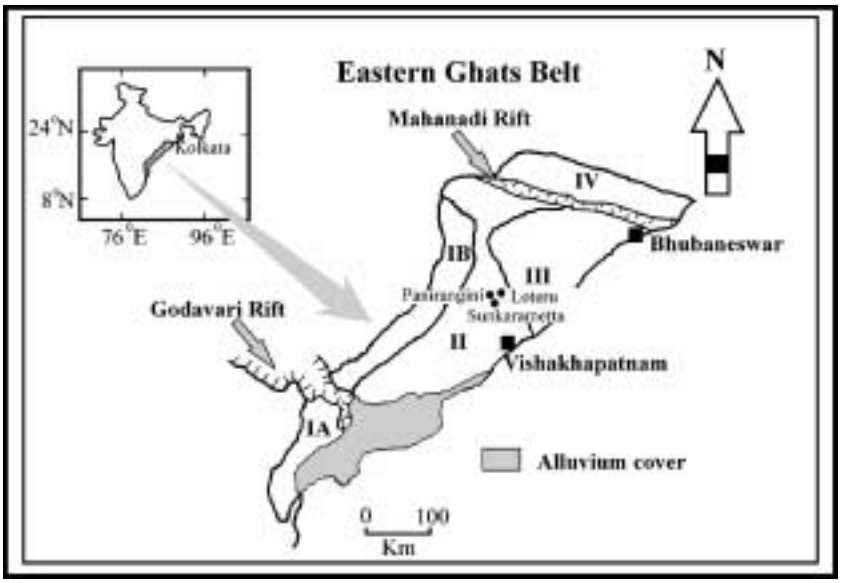

Fig. 1. Location map of the three studied areas within the Eastern Ghats Belt (EGB), India. Roman letters indicate subdivisions of this belt based on isotopic signatures after Rickers et al. (2001). Exact geographic locations of these three areas are given in the text.

(200–250 m in the long dimension) are hosted by pelitic gneiss (quartz–K–feldspar–plagioclase–garnet–sillimanite) that is fringed by mafic granulite and enderbitic gneiss (Bose et al., 2000, 2003). Samples for the present study (SS) were collected from a massive variety of the aluminous granulites. At Loteru, aluminous granulite enclaves, 3–5 m in the long dimension, occur in leptynitic gneiss (quartz–K–feldspar–plagioclase–garnet) and pelitic gneiss. Two varieties of aluminous granulites are studied here—one a massive (Sample 9d) another a foliated one (Sample Lnd). The foliated variety is distinctly migmatitic with quartzofeldspathic leucosomes (quartz+mesoperthite+plagioclase) alternating with dark layers (garnet+orthopyroxene+ilmenite). The leptynitic host gneiss is fringed by an enderbitic gneiss. At Panirangini, a small (few meters in long dimension) enclave of aluminous granulite occurs in leptynitic gneiss. Aluminous granulites therefore have similar mode of occurrence in all the three areas.

The focus of the present communication is different types of mineral intergrowths in porphyroblastic orthopyroxene in the aluminous granulites. Table 1 represents the summary of the mineral assemblages developed during prograde and retrograde stages and the nature of the intergrown phases. The SS samples contain a granoblastic mosaic of orthopyroxene+cordierite+sapphirine+plagioclase, presumably representing the peak metamorphic assemblage (Bose et al., 2000; Association A). Locally, orthopyroxene forms monomineralic aggregates, which contain abundant intergrowth textures described in the following section. In the 9d samples, the peak assemblage is again represented by orthopyroxene+cordierite+sapphirine+plagioclase+quartz. Orthopyroxene forming massive aggregates contains several types of intergrowths described later. Orthopyroxene+garnet+quartz+plagioclase+ilmenite forms a granoblastic aggregate representing the peak metamorphic assemblage in the Lnd samples. But for the highly aluminous nature of orthopyroxene, this rock resembles a charnockite, and is similar to one of the quartzofeldspathic gneiss sample described by Harley (1985) from the Tula Mountains. In the Pan samples, the porphyroblastic assemblage is of orthopyroxene+cordierite+sapphirine+sillimanite+quartz. Therefore, in all the studied samples orthopyroxene is a constituent of the porphyroblastic phases presumably representing the peak metamorphic assemblage. Decomposition of orthopyroxene, as described in the subsequent sections, is a consequence of post-peak re-equilibration. The Pan samples are presumably true metapelitic granulites with prismatic sillimanite as a constituent of the peak assemblage. The other samples could represent semi-pelitic bulk composition in which sillimanite is present as a coronal phase developed during retrogression (see Bose et al., 2000, 2003).

Table 1
A summary of samples showing different mineral assemblages and intergrowth types

Sample no.	Mineral assemblages		Intergrowth(s) present
	Peak stage	Retrograde stage	
9d_1d	Opx+Crd+Qtz+Pl+Spl+Rt	Opx+Sil+Bt	A-1, C
9d_u_2	Opx+Crd+Qtz+Pl+Rt	Opx+Sil+Bt+Qtz	A-1
9d	Opx+Crd+Spr+Pl+Qtz	Opx+Sil+Bt+Qtz	A-1
9d_6	Opx+Crd+Pl+Qtz+Kfs	Opx+Sil+Bt+Qtz	A-1, C
9d_2	Opx+Crd+Pl+Qtz+Spl	Opx+Sil+Bt+Qtz	B-1
9d_3_3	Opx+Crd+Pl+Rt+Qtz	Opx+Sil+Bt+Qtz	A-1
9d_3B	Opx+Crd+Pl+Qtz	Opx+Sil+Bt+Qtz	A-1
9d_2–3	Opx+Crd+Pl+Qtz	Sil+Bt+Qtz+Opx	B-1, B-3
9d_4_1	Opx+Crd+Spr+Rt+Pl+Spl	Opx+Sil+Bt	C, A-1
9d_2_1	Opx+Kfs+Qtz+Crd	Opx+Sil+Bt	B-1
9d_4	Opx+Spr+Spl+Crd+Pl+Qtz	Opx+Sil+Bt+Qtz	A-1
9d_5B	Opx+Crd+Qtz+Pl+Spl+Rt	Opx+Sil+Bt+Qtz	A-1
9d_3_4	Opx+Spr+Spl+Crd+Pl+Qtz	Opx+Sil+Grt+Bt+Qtz	C
Lnd_1	Opx+Grt+Kfs+Pl+Qtz+Ilm	Grt+Qtz+Bt+Spl+Spr	D
Lnd_2	Opx+Grt+Kfs+Pl+Qtz+Ilm+Spl	Grt+Qtz+Bt+Spl+Spr+Ilm	D
Pan10B	Opx+Spl+Qtz+Grt+Rt+Ilm+Crd	Opx+Sil+Qtz+Crd+Bt	B-2
Pan9A	Opx+Spl+Qtz+Pl+Crd	Opx+Sil+Crd+Qtz	B-1
P9A	Opx+Spr+Qtz+Crd+Sil	Opx+Sil+Crd+Qtz	B-1
Pan9B	Opx+Spr+Pl+Qtz+Crd+Rt	Opx+Sil+Crd+Qtz	B-2
SS5/1	Opx+Spr+Crd+Qtz+Ilm+Pl	Opx+Sil+Bt+Qtz	A-1, A-2
SS3/2	Opx+Crd+Pl+Kfs+Qtz	Opx+Sil+Bt+Qtz	C
SS97	Opx+Grt+Qtz+Ilm+Pl	Grt+Qtz+Bt+Ilm	D

3. The intergrowths: texture and mineral chemistry

The focus of this communication is the presence of various types of mineral intergrowths mostly within the orthopyroxene porphyroblasts. Fig. 2 shows the nature

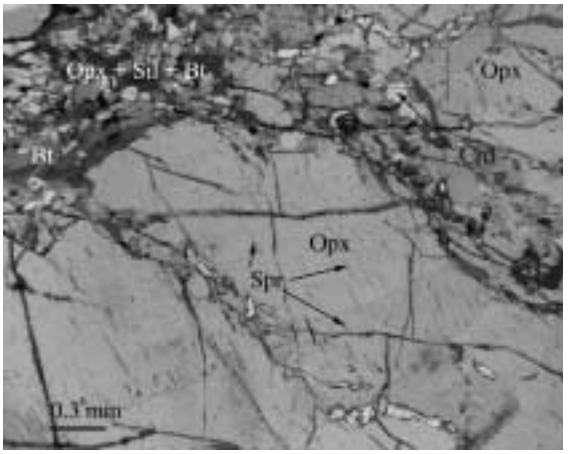

Fig. 2. Photomicrograph showing coarse orthopyroxene (Opx) containing oriented lamellae of sapphirine (Spr) along crystallographic direction. The surrounding matrix is composed of cordierite (Crd) and an intergrowth of orthopyroxene, sillimanite and biotite (Opx+Sil+Bt).

of sapphirine lamellae in megacrystic orthopyroxene, deflected around by a foliation defined by granular orthopyroxene and sillimanite in an aluminous granulite. Cordierite porphyroblasts occur in the matrix and biotite locally replaces orthopyroxene. In rare circumstances, the intergrown phase also occurs surrounding the orthopyroxene grains. The intergrowths are classified according to the key minerals in each.

A. Intergrowth involving sapphirine
B. Intergrowth involving spinel, but without sapphirine
C. Intergrowth involving cordierite, but without sapphirine and spinel
D. Intergrowth involving garnet, without sapphirine, spinel or cordierite.

3.1. A-type intergrowth involving sapphirine

These intergrowths are characterized by sapphirine as the ubiquitous phase. This can be further subdivided into:

A-1: Sapphirine±quartz±spinel±ilmenite
A-2: Sapphirine-cordierite

The A-1 type intergrowth is commonly found in samples SS and 9d. In both the samples, sapphirine forms thin lamella in orthopyroxene along crystallographic directions (Fig. 3a). In SS samples, sapphirine also forms patches in orthopyroxene (Fig. 3b), which was reported earlier by Bose et al. (2000). Rarely, however, sapphirine forms symplectic intergrowth with quartz. Here, coarse orthopyroxene show very delicate symplectite of sapphirine and quartz with minor orthopyroxene (Fig. 3c). Similar textural feature was described by Harley and Motoyoshi (2000). Locally, lamellae of spinel and ilmenite occur in orthopyroxene (Fig. 3c). Ilmenite laths intergrown with orthopyroxene were earlier described by Schulze et al. (1978) from pyroxenite xenoliths.

Mineral chemical analysis was carried out with JEOL-JXA-8900 Electron Microprobe Analyzer at the Hiroshima University and with JEOL-733 Electron Microprobe Analyzer at Hokkaido University, Japan both with the operating condition of 15 kV accelerating voltage, 20 nA beam current and 1–2 μm beam diameter. All the elements except Zn are measured using synthetic standards. For Zn, we used ASTM standard mineral willemite.

Representative compositional data of the A-type intergrowths are given in Table 2. Compositions of representative phases are plotted in the S-BF-BM projection plane following the method outlined by McDade and Harley (2001) (Fig. 4a). Sapphirine in the samples 9d and SS is magnesian (X_{Mg}=0.75–0.80). Ferric iron content in sapphirine was calculated by stoichiometric balancing after the method of Grew (pers. comm.) and these show considerable inter-sample variations. Cr content in sapphirine is low (Cr_2O_3=0.1–0.3 wt.%). All the grains are peraluminous and plot in linear array close to the line joining 7:9:3 and 2:2:1, being closer to the former (Fig. 5). There is no major compositional difference between A-1 and A-2-type sapphirine in the same orthopyroxene host. Host orthopyroxene grains (X_{Mg}=0.69–0.70) in the 9d samples are aluminous and show marked decrease in alumina from intergrowth-free regions (9.9 wt.%) to regions close to sapphirine lamellae or vein (8.5 wt.%), although no significant zoning in Fe–Mg is discernable. Orthopyroxene grains in the SS samples are compositionally similar, particularly in terms of Fe–Mg (X_{Mg}=0.67–0.71). Alumina content also shows marked decrease from intergrowth-free regions (10.2 wt.%) to regions near sapphirine (8.7 wt.%). Orthopyroxene in the A-1 intergrowth is relatively more aluminous than that in the A-2 type (Fig. 6). Orthopyroxene contains 0.4–1.4 wt.% Fe_2O_3 on recalculation. Spinel is magnesian (X_{Mg}=0.48) and recalculated composition shows presence of appreciable Fe_2O_3 (2.6–3.2 wt.%). It contains small amount of ZnO (0.9–1.1 wt.%) and insignificant amount of Cr_2O_3 (0.2 wt.%). Recalculated composition shows 46–47 mol% spinel, 49 mol% hercynite, 2–3 mol%

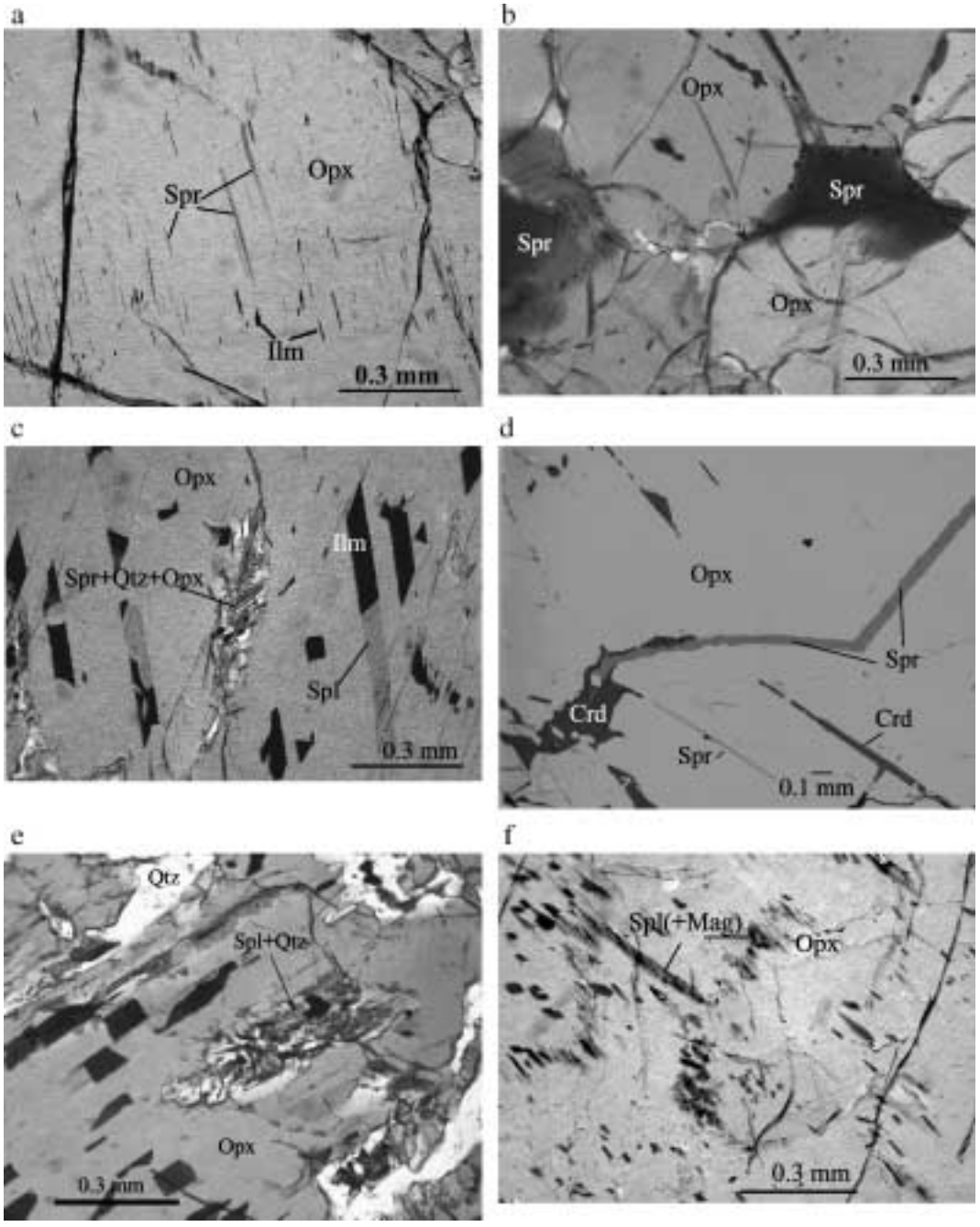

Fig. 3. Photomicrographs and back-scattered electron (BSE) images showing the relation of host orthopyroxene and different intergrown phases. (a) Sapphirine (Spr) and ilmenite (Ilm) lamellae along crystallographic orientation of the host orthopyroxene (Opx) in 9d sample. (b) Sapphirine (Spr) patches at the grain margin of porphyroblastic orthopyroxene (Opx) in SS sample. (c) Delicate symplectite consisting of sapphirine, quartz and minor orthopyroxene (Spr+Qtz+Opx) in porphyroblastic orthopyroxene (Opx) in SS sample. Note the presence of ilmenite (Ilm) and spinel (Spl) needles along crystallographic orientation. (d) BSE image of SS sample showing the presence of thin sapphirine (Spr) vein and cordierite (Crd) in orthopyroxene (Opx) host. Thin cordierite and sapphirine lamellae are also present along the crystallographic orientation in the host. (e) Vermicular intergrowth of spinel and quartz (Spl+Qtz) forms at the interior of orthopyroxene (Opx) in Pan sample. Associated grains are quartz (Qtz). (f) Irregular blebs of spinel (Spl) with exsolved magnetite in host orthopyroxene in 9d sample. (g) Lamellar intergrowth of garnet (Grt) and spinel (Spl) along crystallographic direction in fractured host orthopyroxene (Opx) in Pan sample. (h) Spinel (Spl) and cordierite (Crd) form separate lamellae, but are oriented along the same crystallographic plane of host orthopyroxene (Opx) in SS sample. (i) BSE image of SS sample showing oriented lamellae of cordierite (Crd) and ilmenite (Ilm) in host orthopyroxene (Opx) grain. (j) Garnet (Grt) forms extensive lamellae in host orthopyroxene (Opx) in Lnd sample.

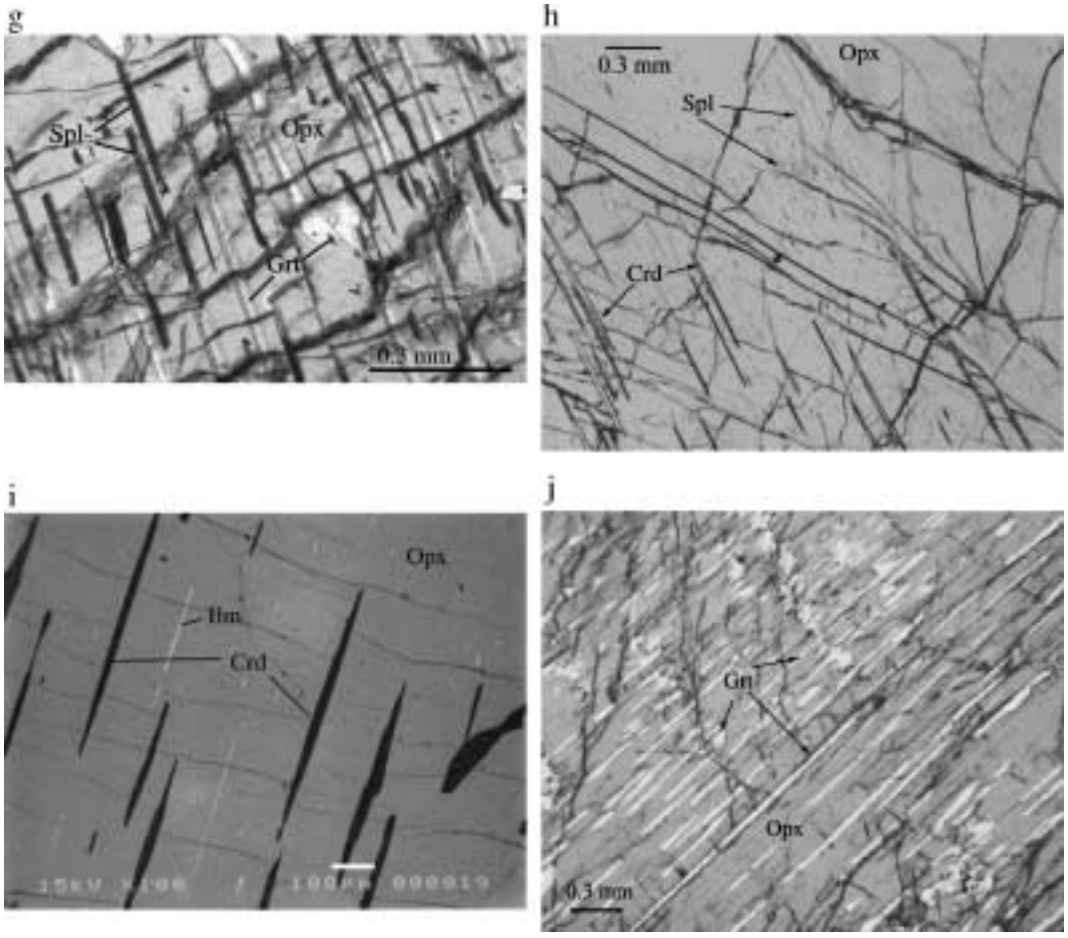

Fig. 3 (*continued*).

magnetite and 2 mol% gahnite components. Ilmenite contains 80–81 mol% ilmenite, 10 mol% hematite and 9–10 mol% geikielite components.

The A-2 type intergrowth is observed in orthopyroxene in the SS samples. In most of the cases, sapphirine occurs as thin veins at the mutual boundaries of orthopyroxene grains with an even thinner skin of cordierite (Fig. 3d). This intergrowth is observed in domains composed of orthopyroxene (modally 90%) and cordierite (modally 10%). Sapphirine and cordierite also occur as lamellae in the same orthopyroxene grain (Fig. 3d).

Sapphirine is magnesian and compositionally homogeneous (X_{Mg}=0.75–0.76). Ferric iron content in such grains is fairly high (2.6–3.1 wt.% Fe_2O_3; X^{3+}_{Fe}=0.21–0.24). All the compositions plot close to the Tschermak substitution line (Fig. 5). Cordierite is homogeneous in composition (X_{Mg}=0.86). Host orthopyroxene is magnesian (X_{Mg}=0.67–0.70) and shows significant drop in alumina content from intergrowth-free regions (10.6 wt.%) to regions adjacent to sapphirine and cordierite (8.2 wt.%). All the phases contain small but variable amount of ferric iron (0–1.5 wt.% Fe_2O_3).

3.2. B-type intergrowths involving spinel

Intergrowths involving spinel but without sapphirine are widespread in orthopyroxene in almost all the studied samples. However, there are mineralogical variations in the participating phases and therefore, these are described under the following subheadings:

B-1: Spinel and ilmenite
B-2: Spinel and garnet
B-3: Spinel and cordierite.

The B-1 type intergrowth is widespread in the SS, Pan, and 9d samples. Green spinel (with or without ilmenite) occurs as crystallographically oriented thin needles and plates in orthopyroxene megacrysts in SS

Table 2
Representative composition of host orthopyroxene and the intergrown phases in A-type intergrowth

Type	A-1												A-2			
Phase	Opx	Opx	Spr	Opx	Opx	Spr	Opx	Opx	Spr	Ilm	Spl		Opx	Opx	Spr	Crd
Sample no.	9d_1d	9d_1d	9d_1d	SS5/1	SS5/1	SS5/1	9d_u2	9d_u2	9d_u2	9d_u2	9d_u2		SS5/1	SS5/1	SS5/1	SS5/1
Texture type	Ifr	Cti		Ifr	Cti		Ifr	Cti					Ifr	Cti		
SiO_2	47.97	49.03	12.97	48.28	48.09	13.47	48.31	48.67	13.33	0.04	0.02		48.04	48.83	13.38	49.61
TiO_2	0.20	0.18	0.05	0.18	0.16	0.03	0.20	0.16	0.13	51.09	0.01		0.22	0.11	0.04	–
Al_2O_3	9.89	8.51	60.81	10.19	8.67	59.47	9.42	8.79	59.00	0.05	61.46		10.63	8.20	59.56	33.33
Cr_2O_3	0.01	0.05	0.09	–	–	–	0.01	0.04	0.07	0.02	0.22		–	–	–	–
Fe_2O_3	1.16	0.91	2.27	0.37	1.36	2.56	1.42	1.78	2.72	–	2.61		0.02	1.54	2.71	–
FeO	17.80	17.82	7.53	18.24	17.62	8.60	17.94	17.70	8.20	46.10	22.48		18.78	18.06	8.59	3.33
MnO	0.20	0.15	0.05	0.27	0.25	0.08	0.14	0.16	0.12	0.23	0.11		0.21	0.29	0.09	0.05
MgO	22.12	22.72	15.56	22.00	22.76	15.25	22.26	22.62	15.31	2.67	11.85		21.60	22.40	15.20	11.28
CaO	0.08	0.25	0.02	0.13	0.12	–	0.14	0.13	0.05	–	0.02		0.11	0.12	–	–
ZnO	–	–	–	–	–	–	–	–	–	–	1.03		–	–	–	–
Na_2O	–	–	–	–	–	–	–	–	–	–	–		–	–	–	0.02
Total	99.44	99.62	99.38	99.66	99.84	99.46	99.83	100.05	98.93	100.21	99.81		99.61	99.45	99.57	97.62
O-basis	6	6	10	6	6	6	6	6	10	3	4		6	6	10	18
Si	1.764	1.798	0.782	1.770	1.790	0.82	1.771	1.781	0.812	0.001	0.001		1.764	1.798	0.810	5.022
Ti	0.006	0.005	0.002	0.005	0.005	0.00	0.005	0.005	0.006	0.946	–		0.006	0.003	0.002	–
Al	0.429	0.368	4.323	0.440	0.374	4.25	0.407	0.379	4.236	0.001	1.941		0.460	0.356	4.252	3.977
Cr	–	0.001	0.004	–	–	–	–	0.001	0.003	–	0.005		–	–	–	–
Fe^{3+}	0.032	0.025	0.103	0.010	0.037	0.117	0.039	0.049	0.125	0.105	0.053		–	0.043	0.124	–
Fe^{2+}	0.548	0.547	0.380	0.559	0.539	0.436	0.550	0.542	0.418	0.844	0.504		0.577	0.556	0.435	0.282
Mn	0.006	0.005	0.003	0.008	0.008	0.004	0.004	0.005	0.006	0.005	0.003		0.007	0.009	0.005	0.004
Mg	1.212	1.242	1.399	1.202	1.242	1.378	1.217	1.234	1.391	0.098	0.473		1.182	1.230	1.373	1.702
Ca	0.003	0.010	0.003	0.005	0.005	–	0.005	0.005	0.003	–	0.001		0.004	0.005	–	–
Zn	–	–	–	–	–	–	–	–	–	–	0.020		–	–	–	–
Na	–	–	–	–	–	–	–	–	–	–	–		–	–	–	0.004
Total	4.000	4.000	7.000	4.000	4.000	7.000	4.000	4.000	7.000	2.000	3.000		4.000	4.000	7.000	10.991
X_{Mg}	0.69	0.69	0.79	0.68	0.70	0.76	0.69	0.69	0.77	–	0.48		0.67	0.69	0.76	0.86
X^{3+}_{Fe}	0.06	0.04	0.21	0.02	0.06	0.21	0.07	0.08	0.23	0.11	0.09		–	0.07	0.22	–
											X_{Mag}	0.03				
									X_{Ilm}	0.81	X_{Hc}	0.49				
									X_{Hem}	0.10	X_{Gah}	0.02				
									X_{Gk}	0.09	X_{Spl}	0.46				

– Below detection limit.
Ifr = intergrowth-free region, Cti = close to intergrowth.

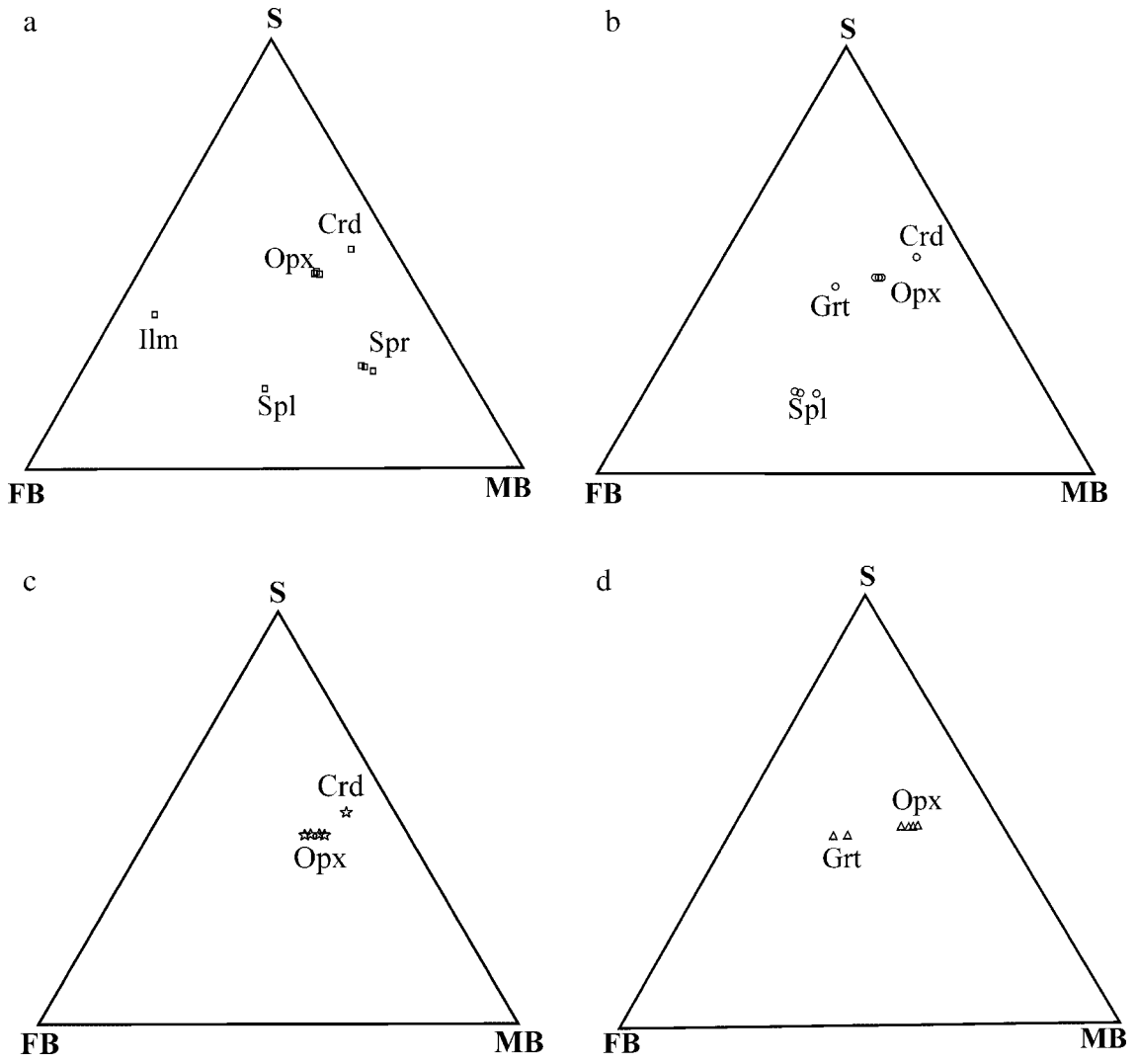

Fig. 4. S-FB-MB projective plots of host and different intergrown phases in (a) A-type, (b) B-type, (c) C-type and (d) D-type intergrowths after the method outlined by McDade and Harley (2001).

samples, and as spinel-quartz vermicular symplectite in orthopyroxene in Pan samples (Fig. 3e). Spinel also forms irregular patches and blebs at the mutual grain boundaries of orthopyroxene (Fig. 3f). Green spinel contains small blebs of exsolved magnetite in all such occurrences, thereby suggesting early stabilization of a Fe-rich spinel solid solution.

The compositional data of the phases are presented in Table 3 and shown in Fig. 4b in S-BF-MF plot. Spinel is rich in hercynite component and X_{Mg} varies from 0.34 to 0.38, which is significantly lower than that in A-1. Recalculation shows 2–5 wt.% Fe_2O_3. ZnO content is low (1.1–1.5 wt.%) and TiO_2 and Cr_2O_3 contains are insignificant (<0.1 wt.%). Compositionally spinel is 34–39 mol% spinel, 57–61 mol% hercynite, 2–5 mol% magnetite and 2–3 mol% gahnite. Host orthopyroxene is less magnesian (X_{Mg}=0.63–0.64) as compared to those containing sapphirine. It is again highly aluminous and the alumina content drops significantly from intergrowth-free portions (9.6 wt.%) to areas near spinel (8.9 wt.%). Fe_2O_3 content is variable (0.3 to 3.0 wt.%) while Cr_2O_3 is insignificant (<0.01 wt.%).

The B-2 type rare intergrowth is found in the Pan samples. Most of the orthopyroxene grains are intergrowth-free, but some contain lamellae of garnet and spinel (with magnetite) along a crystallographic plane within the same grain (Fig. 3g). Spinel is slightly more magnesian (X_{Mg}=0.43) than those in B-1 type. Recalculated composition shows 2.5 wt.% Fe_2O_3. ZnO content is slightly higher (1.94 wt.%) than those of B-1

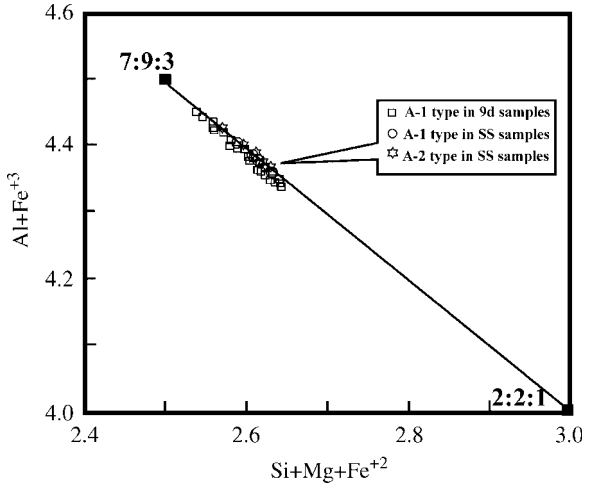

Fig. 5. Compositional plot of sapphirine in ($Al+Fe^{3+}$) vs. ($Si+Mg+Fe^{2+}$) space after Grew (pers. comm.). All the sapphirine grains in A-1 and A-2 type intergrowths plot in a linear array along the line joining 7:9:3 and 2:2:1 compositions. Note, however, all the compositions plot closer to the 7:9:3 point.

type. Compositionally spinel is 40 mol% spinel, 53 mol % hercynite, 3 mol% magnetite and 4 mol% gahnite. Garnet contains 46 mol% pyrope, 52 mol% almandine with small amount of grossular and spessartine. Host orthopyroxene contains 8.7 wt.% Al_2O_3 in the intergrowth-free portion that drops down to 7.9 wt.% near spinel and garnet lamellae. X_{Mg} (0.64–0.65) is nearly constant and same as that in the B-2 type.

The B-3 type intergrowth is noted only in a few SS and 9d samples. Blebs and lamellae of spinel and cordierite are oriented separately along the same crystallographic direction in a single grain of megacrystic orthopyroxene (Fig. 3h). Additionally, the intergranular space between adjacent orthopyroxene porphyroblasts that form aggregates is occupied by spinel and cordierite. In such occurrences, cordierite forms thin to thick corona on spinel.

Spinel (X_{Mg}=0.39) is rich in hercynite component (57 mol%) with small amounts of magnetite (3 mol%) and gahnite (3 mol%). Cordierite is comparatively less magnesian (X_{Mg}=0.82) than that in the A-2 type (see Table 2). Host orthopyroxene is homogeneous in terms of Fe–Mg distribution (X_{Mg}=0.62–0.63), but is less magnesian than that in the A-2 type. Small-scale Al-zoning is observed from intergrowth-free region (9.1 wt.%) to areas close to spinel and cordierite (8.9 wt.%).

3.3. C-type intergrowth involving cordierite–ilmenite

This type of intergrowth is common in the SS, 9d and Lnd samples. Orthopyroxene, coexisting with porphyroblastic cordierite and plagioclase as the peak metamorphic assemblage in microdomains, contains lamellae of cordierite and ilmenite along a crystallographic plane. These lamellae taper at both ends (Fig. 3i).

Representative analytical data are given in Table 4 and the data are plotted on S-BF-BM plane in Fig. 4c. Cordierite is highly magnesian (X_{Mg}=0.82–0.87) in all the samples and may contain up to 0.04 wt.% Na_2O. Host orthopyroxene grains in the different occurrences show variable X_{Mg} (0.61–0.71), but in each case show sharp drop in alumina content at the contact of the intergrown cordierite (ΔAl_2O_3=0.6 wt.%).

3.4. D-type intergrowth involving garnet–ilmenite

This distinctive texture is found in a few SS and Lnd samples. Garnet with/without ilmenite occur as irregular veins and lamellae in orthopyroxene and also forms thin corona on the latter (Fig. 3j). Representative analytical data are given in Table 4. Garnet in the Lnd samples is compositionally $Alm_{54-55}Prp_{40-42}Grs_{3-4}Sps_1$. Garnet in the SS samples is more iron-rich ($Alm_{57}Prp_{35}Grs_6Sps_2$). The host orthopyroxene varies in composition from X_{Mg}=0.67–0.69 in the Lnd samples and X_{Mg}=0.64–0.71 in the SS samples. In all cases orthopyroxene is aluminous and shows drop in alumina content near the intergrown garnet, e.g. Al_2O_3 wt.% from 8.3 to 7.3 in the Lnd samples and from 6.9 to 5.1 in the SS samples. Recalculation shows the presence of 2.8 wt.% Fe_2O_3 in the Lnd

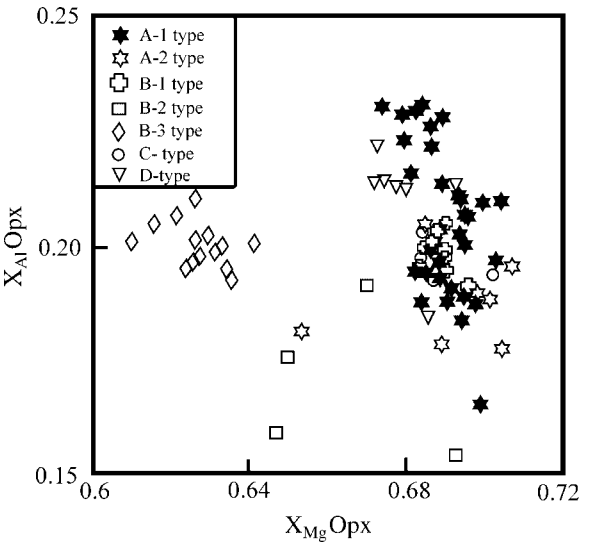

Fig. 6. Compositional plot of orthopyroxene in terms of X_{Mg} [=Mg/(Mg+Fe^{2+})] and X_{Al} (=Al/2) in different types of intergrowths.

Table 3
Representative composition of host orthopyroxene and the intergrown phases in B-type intergrowth

Type	B-1			B-2				B-3			
Phase	Opx	Opx	Spl	Opx	Opx	Spl	Grt	Opx	Opx	Spl	Crd
Sample no.	9d_2	9d_2	9d_2	Pan10B	Pan10B	Pan10B	Pan10B	9d_2	9d_2	9d_2	9d_2
Texture type	Ifr	Cti		Ifr	Cti			Ifr	Cti		
SiO_2	47.12	47.91	–	47.76	48.08	0.02	40.04	47.45	47.59	–	49.26
TiO_2	0.12	0.18	0.04	0.12	0.01	0.09	0.04	0.1	0.13	–	0.23
Al_2O_3	9.61	8.87	59.14	8.67	7.94	60.07	22.46	9.1	8.88	60.22	33.27
Cr_2O_3	–	–	0.08	0.03	0.01	0.05	0.03	0.02	–	0.05	0.02
Fe_2O_3	2.05	2.14	4.48	1.6	1.92	2.49	–	2.4	1.51	3.32	–
FeO	21.05	20.82	26.6	20.44	20.03	23.8	24.98	20.85	21.39	26.01	4.35
MnO	0.16	0.22	0.1	0.06	0.11	0.03	0.29	0.21	0.2	0.11	0.04
MgO	19.77	20.37	8.82	20.55	20.88	10.15	12.34	20.04	19.88	9.22	11.11
CaO	–	0.08	–	0.06	0.12	0.04	0.83	0.02	–	0.01	0.01
ZnO	–	–	1.54	–	–	1.94	–	–	–	1.57	–
Na_2O	–	–	–	–	–	–	–	–	–	–	0.03
Total	99.88	100.59	100.81	99.29	99.09	98.68	101.02	100.19	99.56	100.51	98.1
O-basis	6	6	4	6	6	4	12	6	6	4	18
Si	1.76	1.77	–	1.78	1.80	0	3	1.76	1.78	–	4.99
Ti	0	0.01	0	0	–	0	0	0	0	–	0
Al	0.42	0.39	1.91	0.38	0.35	1.94	1.98	0.39	0.39	1.93	3.97
Cr	–	–	0	0	–	0	0	–	–	0	0
Fe^{3+}	0.06	0.06	0.09	0.05	0.05	0.05	–	0.07	0.04	0.07	–
Fe^{2+}	0.66	0.64	0.61	0.64	0.63	0.55	1.56	0.65	0.67	0.59	0.37
Mn	0.01	0.01	0	0	0	0	0.02	0.01	0.01	0	0
Mg	1.10	1.12	0.36	1.14	1.16	0.42	1.38	1.11	1.11	0.37	1.68
Ca	–	0	–	0	0.01	0	0.07	0	–	–	–
Zn	–	–	0.03	–	–	0.04	–	–	–	0.03	–
Na	–	–	–	–	–	–	–	–	–	–	0.01
Total	4.000	4.000	3.000	4.000	4.000	3.000	8.007	4.000	4.000	3.000	11.024
X_{Mg}	0.63	0.64	0.37	0.64	0.65	0.43	0.47	0.63	0.62	0.39	0.82
X_{Fe}^{3+}	0.08	0.08	0.13	0.07	0.08	0.09	–	0.09	0.06	0.10	–
X_{Mag}			0.04			0.02	X_{Prp} 0.46		X_{Mag}	0.03	
X_{Hc}			0.59			0.53	X_{Alm} 0.52		X_{Hc}	0.57	
X_{Gah}			0.02			0.04	X_{Grs} 0.02		X_{Gah}	0.03	
X_{Spl}			0.35			0.4	X_{Sps} 0.01		X_{Spl}	0.37	

– Below detection limit.
Ifr = intergrowth-free region, Cti = close to intergrowth.

samples, and 3.4–5.3 wt.% Fe_2O_3 in the SS samples. Compositions of different phases are plotted in the S-BF-BM projection plane (Fig. 4d).

4. Peak and retrograde *P–T* conditions

Bose et al. (2000) have deduced the pressure and temperature conditions during the peak stage for the SS samples as ca.8.5+0.5 kbar and >1000 °C. In the other samples (9d, Lnd and Pan), temperatures of >900 °C are obtained from the alumina content of the most aluminous orthopyroxene (>9 wt.% Al_2O_3) in association with sapphirine, garnet, quartz and cordierite according to the data of Harley (1998). The same compositional data, when considered in the phase diagram of Harley (2004) gives 1000–1050 °C for the peak condition. Reintegration of mesoperthite composition occurring in the leucosomes by image analysis in the 9d and Lnd samples gives temperatures close to 1000 °C according to the model of Hokada (2001). The assemblage garnet–orthopyroxene–plagioclase–quartz in the Lnd sample gives 970–980 °C at 9.2–9.3 kbar using the model RCLC of Pattison et al. (2003). We have also employed several ion-exchange thermometers using the intergrowth assemblages. Sapphirine patches and veins in orthopyroxene in the A-1 type intergrowth gives 770–880 °C using the model of Kawasaki and Sato (2002). Garnet lamellae in orthopyroxene in the D-type intergrowth give 790–830 °C at an assumed pressure of 9 kbar, according to the model of Lee and Ganguly (1988). The model of Pattison et al. (2003), which accounts for the late re-

Table 4
Representative composition of host orthopyroxene and the intergrown phases in C- and D-type intergrowths

Type	C									D					
Phase	Opx	Opx	Crd	Opx	Opx	Crd	Opx	Opx	Crd	Opx	Opx	Grt	Opx	Opx	Grt
Sample no.	9d_2	9d_2	9d_2	9d_6	9d_6	9d_6	SS3/2	SS3/2	SS3/2	Lnd_1	Lnd_1	Lnd_1	SS97	SS97	SS97
Texture type	Ifr	Cti		Ifr	Cti		Ifr	Cti		Ifr	Cti		Ifr	Cti	
SiO_2	47.17	47.73	49.41	48.42	48.08	50.03	48.04	48.28	49.63	48.43	49.30	39.63	47.95	49.62	38.59
TiO_2	0.18	0.11	–	0.17	0.17	–	0.18	0.19	–	0.15	0.13	0.08	0.13	0.11	0.05
Al_2O_3	9.42	8.91	33.06	9.09	8.91	33.30	10.13	9.46	33.67	8.30	7.34	22.23	6.94	5.06	21.50
Cr_2O_3	–	–	–	0.03	0.02	–	–	–	–	0.03	0.05	0.07	0.02	0.08	0.08
Fe_2O_3	1.96	1.95	–	1.24	2.07	–	1.93	1.81	–	2.89	2.76	–	3.38	5.35	–
FeO	21.37	20.86	4.16	18.29	16.93	3.63	16.87	17.08	3.40	18.98	18.44	26.06	20.29	17.38	27.92
MnO	0.16	0.14	0.02	0.16	0.21	0.01	0.19	0.29	0.01	0.09	0.19	0.49	0.44	0.20	0.99
MgO	19.66	20.27	11.07	22.16	22.35	11.63	22.67	22.67	11.68	21.79	22.62	11.06	20.52	23.35	9.59
CaO	–	0.03	–	0.08	0.51	0.62	0.08	0.09	0.02	0.10	0.10	1.49	0.11	0.18	2.20
ZnO	–	–	0.06	–	–	0.05	–	–	–	–	–	–	–	–	–
Na_2O	–	–	0.04	–	–	0.03	–	–	0.02	–	–	–	–	–	–
Total	99.92	100.00	97.76	99.63	99.25	98.74	100.09	99.87	98.46	100.77	100.91	101.15	99.78	101.33	100.92
O - basis	6	6	18	6	6	18	6	6	18	6	6	12	6	6	12
Si	1.760	1.774	5.016	1.781	1.773	5.019	1.751	1.766	4.988	1.776	1.800	2.991	1.795	1.813	2.961
Ti	0.005	0.003	–	0.005	0.005	–	0.005	0.005	–	0.004	0.004	0.005	0.004	0.003	0.003
Al	0.414	0.391	3.956	0.394	0.387	3.938	0.435	0.408	3.998	0.359	0.316	1.976	0.306	0.218	1.945
Cr	–	–	–	0.001	0.001	–	–	–	–	0.001	0.001	0.004	0.001	0.002	0.005
Fe^{3+}	0.055	0.054	–	0.034	0.057	–	0.053	0.050	–	0.080	0.076	–	0.095	0.147	–
Fe^{2+}	0.667	0.648	0.352	0.562	0.522	0.304	0.514	0.523	0.286	0.582	0.563	1.644	0.635	0.531	1.792
Mn	0.005	0.004	0.002	0.005	0.007	0.002	0.006	0.009	0.001	0.003	0.006	0.032	0.014	0.006	0.065
Mg	1.093	1.123	1.676	1.215	1.229	1.738	1.232	1.236	1.750	1.191	1.231	1.243	1.145	1.272	1.097
Ca	–	0.001	–	0.003	0.020	0.005	0.003	0.004	0.002	0.004	0.004	0.120	0.004	0.007	0.181
Zn	–	–	0.001	–	–	0.004	–	–	–	–	–	–	–	–	–
Na	–	–	0.007	–	–	0.006	–	–	0.004	–	–	–	–	–	–
Total	4.000	4.000	11.010	4.000	4.000	11.016	4.000	4.000	11.023	4.000	4.000	8.015	4.000	4.000	8.048
X_{Mg}	0.62	0.63	0.83	0.68	0.7	0.85	0.71	0.7	0.86	0.67	0.69	0.43	0.64	0.71	–
X^{3+}_{Fe}	0.08	0.08	–	0.06	0.1	–	0.09	0.09	–	0.12	0.12	–	0.13	0.22	0.38
X_{Prp}												0.41			0.35
X_{Alm}												0.54			0.57
X_{Grs}												0.04			0.06
X_{Sps}												0.01			0.02

– Below detection limit.
Ifr = intergrowth-free region, Cti = close to intergrowth.

equilibration of Fe–Mg during retrogression, gives much higher temperature estimates (970–1020 °C) using the same compositions.

5. Origin of the microtextures

The occurrence of various phases as lamellar and other forms of intergrowth in orthopyroxene is intriguing. Occurrence of lamellar intergrowth in orthopyroxene can most commonly be explained by the mechanism of exsolution. There are ample natural data on exsolved lamellae of garnet and plagioclase in orthopyroxene from mantle-derived ultramafites and anorthositic rocks (Dymek and Gromet, 1984; Jaffe and Schumacher, 1985 and references therein). In case of these rocks the host orthopyroxene is never as aluminous in pelitic aluminous granulites studied here. Jaffe and Schumacher (1985) concluded that exsolution of garnet from orthopyroxene took place at pressures of around 11 kbar, which is considerably higher than the peak conditions in the study area. Further, the grossular-rich garnet of Jaffe and Schumacher (1985) contrasts sharply with the garnet lamella described here. Harley (1985) described lamellae of garnet and grain-boundary lamella of sapphirine (±rutile) in magnesian and aluminous orthopyroxenes from quartzofeldspathic gneisses. He

explained the formation of the lamellae invoking participation of various Tschermak components in orthopyroxene. In view of the sharp decrease in alumina content of orthopyroxene at the contact with the various types of intergrowths, an attempt is made in the following section to explain their origin through breakdown of several Tschermak components (see Harley, 1985; Hensen, 1988; Nicollet, 1990; Harley and Motoyoshi, 2000; Bose et al., 2000). Such a mechanism was earlier conceived from theoretical (Gasparik, 1994) and experimental (Anastasiou and Seifert, 1972; Arima and Onuma, 1977) studies.

The occurrence of the sapphirine-quartz intergrowth (in type A-1) can be explained by the breakdown of Mg-Tschermak component of orthopyroxene according to the model MAS reaction (Gasparik, 1994)

$$\underset{\text{MgTs}}{2MgAl_2SiO_6} = \underset{\text{Spr (2:2:1)}}{Mg_2Al_4SiO_{10}} + \underset{\text{Qtz}}{SiO_2} \quad (1)$$

However, the presently studied sapphirine lies close to the 7:9:3 composition (Fig. 5) that can be explained by the reaction (Harley and Motoyoshi, 2000)

$$\underset{\text{MgTs}}{9MgAl_2SiO_6} = \underset{\text{Spr (7:9:3)}}{Mg_7Al_{18}Si_3O_{40}} + \underset{\text{En}}{Mg_2Si_2O_6} + \underset{\text{Qtz}}{4SiO_2} \quad (2)$$

With the incorporation of Fe^{2+} in natural rocks, the degree of freedom of these equilibria will be increased by one. The dP/dT slopes of reactions are calculated with the thermodynamic data of Holland and Powell (1998). The dP/dT slope of reaction (2) is 24 bar/K and therefore occurs due to cooling or loading. This reaction was inferred by Harley and Motoyoshi (2000) to explain the occurrence of sapphirine+orthopyroxene+quartz intergrowth after aluminous orthopyroxene during cooling from peak temperature of c. 1120 °C. It is also conceivable that the compositions of coexisting sapphirine and orthopyroxene were affected by the Al-exchange reaction.

MgTs+4 Spr (221)=Spr (793)+En (Harley and Motoyoshi, 2000). The more complex intergrowth of sapphirine+quartz, spinel+ilmenite in Fig. 3c can be produced by a reaction involving breakdown of Fe-Tschermak and FeTi-Tschermak components in addition to Mg-Tschermak component. A possible reaction is

$$\underset{\text{MgTs}}{7MgAl_2SiO_6} + \underset{\text{Fe}^{2+}\text{Ts}}{4FeAl_2SiO_6} + \underset{\text{Fe}^{2+}\text{TiTs}}{3Fe_2TiSio_6} = \underset{\text{Spr(793)}}{Mg_7Al_{18}Si_3O_{40}} + \underset{\text{Herc}}{FeAl_2O_4} + \underset{\text{Ilm}}{3FeTio_3} + \underset{\text{Fs}}{3Fe_2Si_2O_6} + \underset{\text{Qtz}}{5SiO_2} \quad (3)$$

Occurrence of magnetite in spinel can be explained by exsolution from an early-stabilized spinel solid solution during cooling.

Formation of the sapphirine–cordierite intergrowth (A-2) can similarly been explained by breakdown of Mg-Tschermak component (Gasparik, 1994) as

$$\underset{\text{MgTs}}{8MgAl_2SiO_6} = \underset{\text{Spr(2:2:1)}}{3Mg_2Al_4SiO_{10}} + \underset{\text{Crd}}{Mg_2Al_4Si_5O_{18}} \quad (4)$$

This reaction proceeds to the right in response to cooling (Gasparik, 1994). In order to explain the production of sapphirine close to 7:9:3 composition, the following reaction is proposed.

$$\underset{\text{MgTs}}{11MgAl_2SiO_6} = \underset{\text{Spr(7:9:3)}}{Mg_7Al_{18}Si_3O_{40}} + \underset{\text{En}}{Mg_2Si_2O_6} + \underset{\text{Crd}}{Mg_2Al_4Si_5O_{18}} + \underset{\text{Qtz}}{SiO_2} \quad (5)$$

Reaction (5) has a slope of 31.5 bar/K. Therefore, this reaction may proceed towards the right with cooling or loading.

The formation of spinel intergrowth in B-1 can also be explained by the breakdown of Mg-Tschermak component of orthopyroxene (Gasparik, 1994) as

$$\underset{\text{MgTs}}{MgAl_2SiO_6} = \underset{\text{Spl}}{MgAl_2O_4} + \underset{\text{Qtz}}{SiO_2} \quad (6)$$

Spinel in such intergrowths contains abundant magnetite that could have resulted due to exsolution from a pristine Fe-rich spinel$_{ss}$. Alternatively, magnetite can be directly produced along with spinel as a result of breakdown of Fe^{3+}-Tschermak that can be modeled in the FAS system as

$$\underset{\text{Fe}^{2+}\text{Ts}}{FeAl_2SiO_6} + 2\ \underset{\text{Fe}^{2+}\text{Fe}^{3+}\text{Ts}}{FeFe^{3+}AlSiO_6} = 2\ \underset{\text{Herc}}{FeAl_2O_4} + \underset{\text{Mag}}{FeFe_2O_4} + 3\ \underset{\text{Qtz}}{SiO_2} \quad (7)$$

Reaction (6) has dP/dT slope of −22 bar/K and proceeds to the right on decompression with or without cooling.

The B-2 type intergrowth involves both spinel and garnet as product phases and this can be explained by the combined breakdown of Mg-Tschermak and enstatite components of orthopyroxene as

$$\underset{\text{MgTs}}{2MgAl_2SiO_6} + \underset{\text{En}}{Mg_2Si_2O_6} = \underset{\text{Prp}}{Mg_3Al_2Si_3O_{12}} + \underset{\text{Spl}}{MgAl_2O_4} + \underset{\text{Qtz}}{SiO_2} \quad (8)$$

Alternatively, Fe^{3+}-Tschermak component of orthopyroxene can be introduced to account for the occurrence of magnetite in the product

$$(Fe,Mg)Al_2SiO_6 + (Fe,Mg)_2Si_2O_6 + 2FeFe^{3+}AlSiO_6 = (Fe,Mg)_3Al_2Si_3O_{12} + (Fe,Mg)Al_2O_4 + FeFe_2O_{4+}2SiO_2 \quad (9)$$

Reaction (8) has a dP/dT slope of 11 bar/K and may result from cooling and/or loading.

The B-3 type intergrowth containing spinel with cordierite can be explained by another Mg-Tschermak breakdown reaction

$$\underset{MgTs}{5MgAl_2SiO_6} = \underset{Spl}{3MgAl_2O_4} + \underset{Crd}{Mg_2Al_4Si_5O_{18}} \quad (10)$$

Reaction (10) has −0.5 bar/K dP/dT slope and results due to decompression.

Formation of C-type intergrowth containing cordierite can be explained by breakdown of Mg-Tschermak component in presence of quartz

$$\underset{MgTs}{2MgAl_2SiO_6} + \underset{Qtz}{3SiO_2} = \underset{Crd}{Mg_2Al_4Si_5O_{18}} \quad (11)$$

This reaction has 4.43 bar/K dP/dT slope and results due to decompression.

Occurrence of garnet in D-type intergrowth can be explained by involvement of Mg-Tschermak combined with enstatite

$$\underset{MgTs}{MgAl_2SiO_6} + \underset{En}{Mg_2Si_2O_6} = \underset{Prp}{Mg_3Al_2Si_3O_{12}} \quad (12)$$

This reaction, modeled by Gasparik (1994), has −3.35 bar/K dP/dT slope and occurs due to loading (Das et al., 2006) or heating.

6. Discussion

The occurrence of various intergrowth textures in porphyroblastic highly aluminous orthopyroxene, described earlier, provides an opportunity to examine the thermal condition of metamorphism, given the well known dependence of alumina solubility in orthopyroxene on temperature under crustal conditions (Gasparik, 1994; Harley and Motoyoshi, 2000; Hollis and Harley, 2003; references therein). For this purpose, an attempt is made to obtain 'pre-breakdown' composition of orthopyroxene coexisting with various phases, such as sapphirine, cordierite with or without sillimanite and quartz (SS, 9d and Pan samples) during peak metamorphism.

In order to reintegrate the 'pre-breakdown' composition of orthopyroxene, we have started from the inferred mineral reactions as a working model. We have calculated the modal volume ratios of the product phases using the molar volume data given by Holland and Powell (1998) in each stoichiometrically balanced reaction. Subsequently, we have performed image analyses to compute the actual modal volume ratio of the host orthopyroxene and different intergrown phases (Table 5). The final reintegration for the 'pre-breakdown' orthopyroxene was done from the obtained modal volume ratio of the product phases. One major handicap is that all the product/reactant phases are not necessarily present in the intergrowths, as for example, is the case of quartz as a product in reactions (5)–(9). In such cases, we have taken into consideration of those 'missing' phases and added their composition in actual modal volume ratios predicted by respective reactions. Another constraint of this method is that the volume ratios are calculated using model MAS reactions, while the reintegration is done in a complex system, where the volume ratios are bound to be different. Therefore, this scheme of recalculation can be considered as semi-quantitative.

Reaction (1) produces sapphirine (2:2:1) and quartz having the volume ratio of 100:11. The volume ratio of sapphirine (7:9:3) and quartz produced in reaction (2), on the other hand, is 100:46. The observed modal volume ratio of host orthopyroxene and sapphirine recalculated from image analysis is approximately 94.6:5.4. The recalculated compositions of this 'pre-breakdown' orthopyroxene for each of the intergrowths, based on similar calculations, are given in Table 6. The maximum Al_2O_3 content is estimated to be 13.4 wt.%. The maximum TiO_2 and Fe_2O_3 contents are estimated as 0.17 and 3.1 wt.% respectively (Table 6).

Experimental data in the system MAS reveal that Al_2O_3 content in orthopyroxene in association with sapphirine, sillimanite or quartz increases with temperature (Anastasiou and Seifert, 1972; Arima and Onuma, 1977; Danckwerth and Newton, 1978; Hollis and Harley, 2003). Gasparik (1994) calculated the Al-isopleths in orthopyroxene in association with sapphirine+quartz, sapphirine+cordierite, sapphirine+sillimanite and spinel+cordierite in the MAS system. He suggested that a change of 1 wt.% in Al_2O_3 in orthopyroxene would signify a change of 100 °C for these assemblages. This is considered to be an overestimate (Hensen and Harley, 1990; Carrington and Harley, 1995; Aranovich and Berman, 1997), and recent experimental data in the MAS system shows that the temperature change per 1 wt.% change in Al_2O_3 is

Table 5
Calculated ratio of different intergrown phases in different intergrowth types

Sample No	Intergrowth type	Reaction in MAS system	Slope (bar/K)	Volume ratio of phases after MAS reaction	Actual ratio after image analyses
9d_2	A-1	9MgTs=Spr(793)+En+4 Qtz	24.30	Spr:Qtz=2.17	Opx:Spr:Qtz=92.35:5.24:2.41
SS5/1	A-2	11MgTs=Spr(793)+En+Crd	31.50	Spr:Crd=0.85	Opx:Spr:Crd=91.98:3.68:4.34
9d_2	B-1	MgTs=Spl+Qtz	−22.00	Spl:Qtz=1.75	Opx:Spl:Qtz=90.18:6.0:3.82
Pan10B	B-2	2MgTs+En=Prp+Spl+Qtz	11.00	Prp:Spl=2.86	Opx:Grt:Spl:Qtz=86.0:8.96:3.22:1.82
9d_2	B-3	5MgTs=3 Spl+Crd	−0.50	Spl:Crd=0.51	Opx:Spl:Crd=94.24:1.95:3.81
SS3/2	C	2MgTs+3 Qtz=Crd	4.43	Crd:Qtz=3.33	Opx:Crd=95.2:4.8
Lnd_1	D	MgTs+En=Prp	−3.35	Prp:En=1.82	Opx:Grt=91.4:8.6

actually in the order of 25–30 °C (Hollis and Harley, 2003). The obtained 'pre-breakdown' orthopyroxene composition containing a maximum of 13.4 wt.% Al_2O_3 (Table 6) in association with sapphirine+cordierite translates into a maximum temperature of 1300 °C according to the experimentally constrained Al-isopleth diagram (Hollis and Harley, 2003) at a pressure of 8.0+0.5 kbar (Bose et al., 2000). Ultra-high temperatures exceeding 1150 °C (at 8 kbar) are also obtained using the measured maximum Al_2O_3 content in orthopyroxene (9.89 wt.%) coexisting with sapphirine and quartz in the intergrowth A-1 (Sample No. 9d, which contains porphyroblastic sapphirine+quartz in the peak assemblage) using the data of Hollis and Harley (2003). Given the uncertainties in the calculation of pristine orthopyroxene composition and because of the presence of Fe in sapphirine and orthopyroxene, these results are certainly overestimates. The retrieved temperatures from the alumina content of orthopyroxene will be dependent on the Fe^{3+} content in FMASO orthopyroxene. We note that Fe^{3+} is strongly partitioned to sapphirine over orthopyroxene in the studied samples (Table 2), a situation also described by Harley and Motoyoshi (2000). However, unlike the samples from the Napier Complex studied by Harley and Motoyoshi (2000), the EGB samples described here equilibrated at higher fO_2 (discussed in

Table 6
Composition of recalculated orthopyroxene from various intergrowths

Type	A-1		A-2	B-1	B-2	B-3	C		D	
Sample no.	9d_2	SS5/1	SS5/1	9d_2	Pan10B	9d_2	9d_2	SS3/2	Lnd_1	SS97
SiO_2	47.39	47.70	46.83	46.31	46.48	46.59	45.78	46.62	47.67	47.15
TiO_2	0.19	0.17	0.20	0.11	0.11	0.10	0.17	0.17	0.14	0.12
Al_2O_3	12.32	12.53	13.42	12.21	11.40	11.02	10.55	11.26	9.50	8.19
Cr_2O_3	0.01	–	–	–	0.03	0.02	–	–	0.03	0.03
Fe_2O_3	1.19	0.48	0.12	2.12	1.46	2.33	1.87	1.84	2.64	3.09
FeO	16.83	17.30	17.73	20.58	20.58	20.32	20.54	16.22	19.59	20.95
MnO	0.19	0.25	0.20	0.15	0.08	0.20	0.15	0.18	0.12	0.49
MgO	21.24	21.12	20.92	18.36	19.11	19.49	19.25	22.14	20.87	19.58
CaO	0.07	0.12	0.10	–	0.13	0.02	–	0.08	0.22	0.29
Total	99.44	99.66	99.52	99.94	99.44	100.12	98.32	98.51	100.80	99.88
O-basis	6	6	6	6	6	6	6	6	6	6
Si	1.73	1.74	1.71	1.72	1.73	1.73	1.73	1.72	1.75	1.77
Ti	0.01	0.01	0.01	0	0	0	0.01	0.01	0	0
Al	0.53	0.54	0.58	0.54	0.5	0.48	0.47	0.49	0.41	0.36
Cr	–	–	–	–	0	0	–	–	0	0
Fe^{3+}	0.03	0.01	0	0.06	0.04	0.07	0.05	0.05	0.07	0.09
Fe^{2+}	0.51	0.53	0.54	0.64	0.64	0.63	0.65	0.5	0.6	0.66
Mn	0.01	0.01	0.01	0.01	0	0.01	0.01	0.01	0	0.02
Mg	1.16	1.15	1.14	1.02	1.06	1.08	1.09	1.22	1.14	1.1
Ca	0	0.01	0	–	0.01	0	–	0	0.01	0.01
X_{Mg}	0.69	0.69	0.68	0.61	0.62	0.63	0.63	0.71	0.66	0.63
X^{3+}_{Fe}	0.06	0.02	0.01	0.08	0.06	0.09	0.08	0.09	0.11	0.12

– Below detection limit.

details by Bose et al. (2000)). In the system FMAS at high fO_2 the invariant points [Spr], [Crd] and [Grt] are stabilized (Hensen, 1986). The experimentally constrained *P–T* grid of Das et al. (2003) in the system KFMASH at HM buffer is particularly applicable to the studied assemblages. The net result of partitioning of Fe^{3+} in sapphirine over orthopyroxene will be to shift the sapphirine + orthopyroxene (coexisting with various phases such as sillimanite, spinel, cordierite, quartz) fields to lower temperatures along respective (Spr) absent univariant reactions (Figs. 1, 8 in Das et al., 2003) (Harley and Motoyoshi, 2000).

Nevertheless, temperatures exceeding 1000 °C were obtained from the Pattison et al. (2003) Fe–Mg retrieval calculations. Further, the peak metamorphic assemblage of sapphirine + orthopyroxene + cordierite + quartz in the Pan and 9d samples is stable above 1000 °C according to the experimentally constrained petrogenetic grid of Das et al. (2003) in the system KFMASH. Collectively, an extreme thermal condition (>1000 °C) is indicated for the studied rocks.

On the other hand, the difference in alumina content from the 'pre-breakdown' (Table 6) to the present orthopyroxene compositions away from the intergrowths (9.5 to 10 wt.% Al_2O_3) implies a drop of 100–120 °C in temperature according to the data of Hollis and Harley (2003). A further drop of 1–2 wt.% of Al_2O_3 near the intergrowths implies another 30–50 °C fall in temperature. Therefore, cooling over a span of nearly 150 °C is indicated from the breakdown of the pristine orthopyroxenes to the present state. The ΔT estimates are unlikely to be affected by the presence of Fe^{3+} in the coexisting phases (cf. Harley and Motoyoshi, 2000), and may be considered realistic.

The development of diverse types of intergrowths in porphyroblastic orthopyroxene in closely-spaced samples (presumably equilibrated under identical thermobaric conditions) is intriguing. In this connection, it may be recalled that there is a marked difference in the X_{Mg} content of both spinel and orthopyroxene between the intergrowth types A-1 and B-1 (Tables 2 and 3). The A-1 intergrowth involves phases with higher X_{Mg}, and also contains sapphirine lamella. Fig. 7 shows the variation in X_{Mg} of orthopyroxene with X_{Mg} of coexisting phases in the different types of microtextures. The data plot in distinct clusters thereby implying chemical interdependence between the host and guest phases. We are tempted to interpret the clustering in terms of possible bulk rock variations with the A-type intergrowths forming in more magnesian bulk composition.

As discussed by Hollis and Harley (2003), this type of alumina zoning (13.0 wt.% to 9.5 wt.%) in orthopyroxene coexisting with sapphirine and quartz may result from cooling from the peak condition, or loading (along a counterclockwise *P–T* path), or due to superimposition of another UHT event, at lower temperatures or at higher pressures than the first UHT event. The distinction between the two will critically depend on geochronological data in the terrain. The EGB granulites are certainly polymetamorphic, but only the first event of rather uncertain age (Early Proterozoic?) bears the record of UHT metamorphism at temperatures exceeding 1000 °C at 9–10 kbar pressure (Dasgupta and Sengupta, 2003). This UHT event is superimposed successively by a Grenvillian (ca. 1000 Ma; Grew and Manton, 1986; Mezger and Cosca, 1999; Rickers et al., 2001) granulite facies event ("peak" *P–T* conditions of ca. 850–900 °C, 8–8.5 kbar), and an amphibolite facies Pan African (ca. 500 Ma) event (Mezger and Cosca, 1999). The UHT metamorphism in the EGB has a characteristic counterclockwise *P–T* path, as constrained from the prograde part of the *P–T* path (Fig. 8), and post-peak cooling (Sengupta et al., 1990; Dasgupta et al., 1995; Mukhopadhyay and Bhattacharya, 1997). Since there is no evidence of increased pressure during the Grenvillian granulite metamorphism, neither there is any evidence of loading during cooling from the peak UHT conditions of the first event, we consider that the

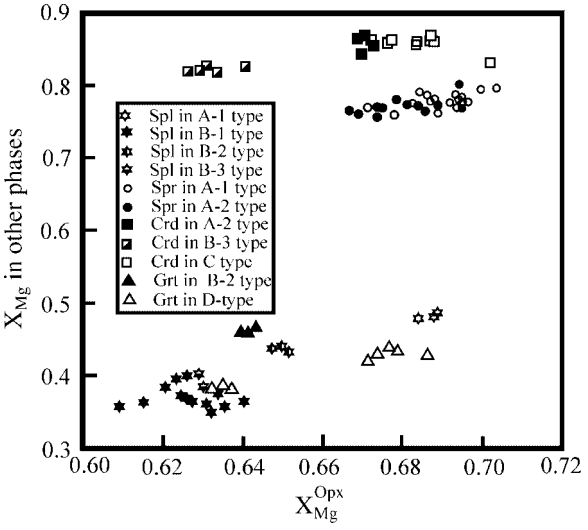

Fig. 7. Plot of X_{Mg} of orthopyroxene with respect to X_{Mg} of other ferromagnesian phases participated in different intergrowths. The plot shows distinct compositional contrasts in different intergrowths suggesting possible contrast in bulk chemistry.

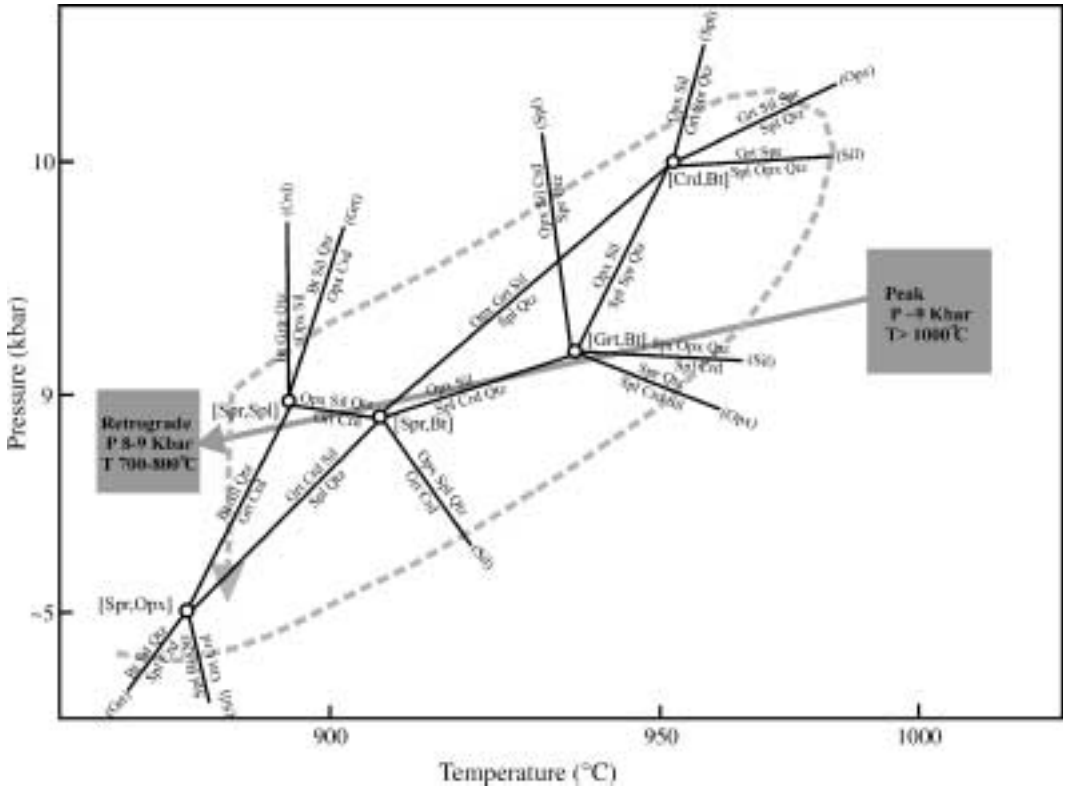

Fig. 8. The petrogenetic grid in the system KFMASH at high fO_2 showing the *P–T* path of evolution (dashed line) of the northern part of the Eastern Ghats Belt (after Dasgupta et al., 1995). The shaded boxes indicate peak and retrograde *P–T* conditions derived from the present study. The solid arrow joining the boxes indicates the approximate evolutionary trend of the studied granulites.

different types of intergrowths in aluminous orthopyroxene described here were produced during cooling from the UHT condition, possibly accompanied by some amount of decompression (Fig. 8).

Acknowledgment

We are thankful to Drs. K. Sajeev and M. Santosh for the invitation to write this paper. SB acknowledges support from the University Grants Commission. KD is thankful to the Ministry of Education, Culture and Sports, Government of Japan for travel and analytical support. H. Nomura and M. Ikeda of Hokkaido University helped during analytical work. SB acknowledges infrastructural support from the FIST program of his department. SD acknowledges financial support from the CAS programme of the Department of Geological Sciences, Jadavpur University. We are thankful to the two journal reviewers (Dr. T. Tsunogae and Dr. S. Baba) for constructive suggestions, and to Profs. M. Santosh and K. Sajeev for efficient editorial handling.

References

Anastasiou, P., Seifert, F., 1972. Solid solubility of Al_2O_3 in enstatite at high temperatures and 1–5 kb water pressure. Contrib. Mineral. Petrol. 34, 272–287.

Aranovich, L.Y., Berman, R.G., 1997. A new garnet–orthopyroxene thermometer based on revised Al_2O_3 solubility in FeO–Al_2O_3–SiO_2 orthopyroxene. Am. Mineral. 82, 345–353.

Arima, M., Onuma, K., 1977. The solubility of alumina in enstatite and the phase equilibria in the join $MgSiO_3$–$MgAl_2SiO_6$ at 10–25 kbar. Contrib. Mineral. Petrol. 61, 251–265.

Bose, S., Fukuoka, M., Sengupta, P., Dasgupta, S., 2000. Evolution of high Mg–Al granulites from Sunkarametta, Eastern Ghats, India: evidence for a lower crustal heating–cooling trajectory. J. Metamorph. Geol. 18, 223–240.

Bose, S., Pal, S., Fukuoka, M., 2003. Pressure–temperature–fluid evolutionary history of orthopyroxene-bearing quartzofeldspathic and mafic granulites from northern parts of the Eastern Ghats Belt, India: implications for Indo-Antarctic correlation. J. Asian Earth Sci. 22, 81–100.

Carrington, D.P., Harley, S.L., 1995. Partial melting and phase relations in high grade metapelites: an experimental petrogenetic grid in the KFMASH system. Contrib. Mineral. Petrol. 120, 270–291.

Danckwerth, P.A., Newton, R.C., 1978. Experimental determination of the spinel peridotite to garnet peridotite reaction in the system MgO–Al2O3–SiO_2 in the range 9000°–1100 °C and Al_2O_3

isopleths of enstatite in the spinel field. Contrib. Mineral. Petrol. 66, 189–201.

Das, K., Dasgupta, S., Miura, H., 2001. Stability of osumilite coexisting with spinel solid solution in metapelitic granulites at high oxygen fugacity. Am. Mineral. 86, 1423–1434.

Das, K., Dasgupta, S., Miura, H., 2003. An experimentally constrained petrogenetic grid in the silica-saturated portion of the system KFMASH at high temperature and pressure. J. Petrol. 44, 1055–1075.

Das, K., Bose, S., Ohnishi, I., Dasgupta, S., 2006. Garnet-spinel intergrowths in ultrahigh-temperature granulite, Eastern Ghats, India: possible evidence of an early Tschermak-rich orthopyroxene during prograde metamorphism. Am. Mineral. 91, 375–384.

Dasgupta, S., 1995. Pressure–temperature evolutionary history of the Eastern Ghats granulite province: recent advances and some thoughts. In: Yoshida, M., Santosh, M. (Eds.), India and Antarctica during the Precambrian. Mem. Geol. Soc. Ind., vol. 34, pp. 101–110.

Dasgupta, S., Sengupta, P., 1995. Ultrametamorphism in Precambrian granulite terrains — evidence from Mg–Al granulites and calc-granulites of the Eastern Ghats, India. Geol. J. 30, 307–318.

Dasgupta, S., Sengupta, P., 2003. Indo-Antarctic correlation: a perspective from the Eastern Ghats Granulite Belt, India. In: Yoshida, M., Windley, B.F., Dasgupta, S. (Eds.), Proterozoic East Gondwana: Supercontinent Assembly and Breakup. Geol. Soc. London Special Publication, vol. 206, pp. 131–143.

Dasgupta, S., Sengupta, P., Ehl, J., Raith, M., Bardhan, S., 1995. Reaction textures in a suite of spinel granulites from Eastern Ghats Belt, India: evidence for polymetamorphism and a partial petrogenetic grid in the system KFMASH and the roles of ZnO and Fe_2O_3. J. Petrol. 36, 435–461.

Dobmeier, C.J., Raith, M.M., 2003. Crustal architecture and evolution of the Eastern Ghats Belt and adjacent regions of India. In: Yoshida, M., Windley, B.F., Dasgupta, S. (Eds.), Proterozoic East Gondwana: Supercontinent Assembly and Breakup. Geol. Soc. London Special Publication, vol. 206, pp. 145–168.

Dymek, R.F., Gromet, L.P., 1984. Nature and origin of orthopyroxene megacrysts from the St, Urbain anorthosite massif, Quebec. Can. Mineral. 22, 297–326.

Fitzsimons, I.C.W., Harley, S.L., 1994. The influence of retrograde cation exchange on granulite P–T estimates and a convergence technique for the recovery of peak metamorphic conditions. J. Petrol. 35, 543–576.

Gasparik, T., 1994. A petrogenetic grid for the system $MgO–Al_2O_3–SiO_2$. J. Geol. 102, 97–109.

Grew, E.S., Manton, W.I., 1986. A new correlation of sapphirine granulites in the Indo-Antarctic metamorphic terrane: Late Proterozoic dates from the Eastern Ghats. Precambrian Res. 33, 123–139.

Harley, S.L., 1985. Garnet-orthopyroxene bearing granulites from Enderby Land, Antarctica: metamorphic pressure–temperature–time evolution of the Archean Napier Complex. J. Petrol. 26, 819–856.

Harley, S.L., 1989. The origin of granulites: a metamorphic perspective. Geol. Mag. 126, 215–247.

Harley, S.L., 1998. On the occurrence and characterisation of ultrahigh-temperature crustal metamorphism. In: Treloar, P.J., O'Brien, P.J. (Eds.), What Drives Metamorphism and Metamorphic Reactions? Geol. Soc. London Special Publication, vol. 138, pp. 81–107.

Harley, S.L., 2004. Extending our understanding of ultrahigh temperature crustal metamorphism. J. Mineral. Petrol. Sci. 99, 140–158.

Harley, S.L., Motoyoshi, Y., 2000. Al zoning in orthopyroxene in a sapphirine quartzite: evidence for 1120 °C metamorphism in the Napier Complex, Antarctica, and implications for the entropy of sapphirine. Contrib. Mineral. Petrol. 138, 293–307.

Hensen, B.J., 1986. Theoretical phase relations involving cordierite and garnet revisited: the influence of oxygen fugacity on the stability of sapphirine and spinel in the system Mg–Fe–Al–Si–O. Contrib. Mineral. Petrol. 92, 362–367.

Hensen, B.J., 1988. Chemical potential diagrams and chemographic projections: applications to sapphirine granulites from Kiranur and Ganguvarpatti, Tamilnadu. Evidence for rapid uplift in part of the South Indian shield? Neues Jahrb. Mineral. Abh. 158, 193–210.

Hensen, B.J., Harley, S.L., 1990. Graphical analysis of *P–T–X* relations in granulite facies metapelites. In: Ashworth, J.R., Brown, M. (Eds.), High Temperature Metamorphism and Crustal Anatexis. Unwin-Hyman, London, pp. 19–56.

Hokada, T., 2001. Feldspar thermometry in ultrahigh-temperature metamorphic rocks: evidence for crustal metamorphism attaining ~1100 °C in the Archean Napier Complex, East Antarctica. Am. Mineral. 86, 932–938.

Holland, T.J.B., Powell, R., 1998. An internally consistent thermodynamic data set for phases of petrological interest. J. Metamorph. Geol. 16, 309–343.

Hollis, J.A., Harley, S.L., 2003. Alumina solubility in orthopyroxene coexisting with sapphirine and quartz. Contrib. Mineral. Petrol. 144, 473–483.

Jaffe, H.W., Schumacher, J.C., 1985. Garnet and plagioclase exsolved from aluminium-rich orthopyroxene in the Marcy Anorthosite, northeastern Adirondacks, New York. Can. Mineral. 23, 457–478.

Kawasaki, T., Sato, K., 2002. Experimental study of Fe–Mg exchange reaction between orthopyroxene and sapphirine and its calibration as a geothermometer. Gondwana Res. 5, 741–747.

Kretz, R., 1983. Symbols for rock forming minerals. Am. Mineral. 68, 277–279.

Lal, R.K., Ackermand, D., Upadhyay, H., 1987. P–T–X relationships deduced from corona textures in sapphirine–spinel–quartz assemblages from Paderu, South India. J. Petrol. 28, 1139–1168.

Lee, H.Y., Ganguly, J., 1988. Equilibrium compositions of coexisting garnet and orthopyroxene: experimental determinations in the system $FeO–MgO–Al_2O_3–SiO_2$ and applications. J. Petrol. 29, 93–113.

McDade, P., Harley, P., 2001. A petrogenetic grid for aluminous granulite facies metapelites in the KFMASH system. J. Metamorph. Geol. 19, 45–59.

Mezger, K., Cosca, M.A., 1999. The thermal history of the Eastern Ghats belt (India), as revealed by U–Pb and 40Ar–34Ar dating of metamorphic and magmatic minerals: implications for the SWEAT correlation. Precambrian Res. 94, 251–271.

Mukhopadhyay, A.K., Bhattacharya, A., 1997. Tectonothermal evolution of the gneiss complex at Salur in the Eastern Ghats Granulite Belt of India. J. Metamorph. Geol. 15, 719–734.

Nicollet, C., 1990. Crustal evolution of the granulites of Madagascar. In: Vielzeuf, D., Vidal, Ph. (Eds.), Granulites and Crustal Evolution. Kluwer Academic Publishers, Netherlands, pp. 291–310.

Pattison, D.R.M., Chacko, T., Farquhar, J., McFarlane, C.R.M., 2003. Temperatures of granulite facies metamorphism: constraints from experimental phase equilibria and thermometry corrected for retrograde exchange. J. Petrol. 44, 867–900.

Rickers, K., Mezger, K., Raith, M.M., 2001. Evolution of the continental crust in the Proterozoic Eastern Ghats Belt, and new constraints for Rodinia reconstruction: implications from Sm–Nd, Rb–Sr and Pb–Pb isotopes. Precambrian Res. 112, 183–212.

Sarkar, S., Santosh, M., Dasgupta, S., Fukuoka, M., 2003. Very high density CO_2 associated with ultrahigh-temperature metamorphism in the Eastern Ghats granulite Belt, India. Geology 31, 51–54.

Schulze, D.J., Helmstaedt, H., Cassie, R., 1978. Pyroxene–ilmenite intergrowths in garnet pyroxenite xenoliths from a New York kimberlite and Arizona latites. Am. Mineral. 63, 258–265.

Sengupta, P., Dasgupta, S., Bhattacharya, P.K., Fukuoka, M., Chakraborti, S., Bhowmick, S., 1990. Petro-tectonic imprints in the sapphirine granulites from Anantagiri, Eastern Ghats Mobile Belt, India. J. Petrol. 31, 971–996.